

Wall Erosion in 2D Hall Thruster Simulations

IEPC-2005-189

Presented at the 29th International Electric Propulsion Conference, Princeton University,
October 31 – November 4, 2005

Emmanuelle Sommier^{*}, Michelle K. Allis[†], and Mark A. Cappelli[‡]
Stanford University, Stanford, CA, 94305

A 2D radial-axial hybrid PIC model has been developed in order to better understand the interactions that occur in Hall thrusters between the plasma and the channel walls. The thruster model geometry corresponds to the Stanford Hall Thruster and the computational domain extends from the anode, through the interior channel, and into the near field plume region. The discharge simulation was carried out for a discharge voltage of 200V and a discharge current of 2.5A. In order to assess thruster degradation due to sputtering, a model of the channel wall erosion process has been added to the simulation as the result of the interaction with the walls of energetic ions and energetic neutrals. The significance of ion-neutral collisions and sheath effects in the erosion process has been studied. These simulations are then used as the basis for computational models that adjust the geometry of the thruster and predict the erosion of the insulator channel walls due to continued sputtering. It was observed that, as the wall is eroded, the erosion rate decreases with time, and that the erosion of the wall reaches 2 to 3 mm after 2000 hours.

Nomenclature

B_r	= radial magnetic field
e	= electron charge
E	= electric field
E^*	= crossover energy
E_c	= energy of a primary electron
E_{Xe^+}	= energy of a Xenon ion
E_z	= axial electric field
g	= relative velocity
$h(z, \varphi, \varepsilon)$	= incident angle and energy distribution function
J	= current density
$J_{e\theta}$	= azimuthal current density
k	= Boltzmann constant
K	= thermal diffusivity
M	= mass
$n_{e,i}$	= plasma/ion density
n_n	= neutral density
r	= radial position
S	= sputter yield
\hat{S}	= normalized sputter yield
T_e	= electron temperature

^{*} Visiting Researcher, Mechanical Engineering Department, emsom@stanford.edu

[†] Research Assistant, Mechanical Engineering Department, mkallis@stanford.edu

[‡] Professor, Mechanical Engineering Department, cap@stanford.edu

z	=	axial position
v	=	velocity
β	=	random number between 0 and 1
χ	=	scattering angle
Φ	=	ion production cost
σ	=	secondary emission electron coefficient
σ_0	=	secondary emission electron coefficient for zero-energy electrons
σ_T	=	total cross section

I. Introduction

Hall thrusters occupy an important place in space propulsion because of their high efficiency compared to chemical engines. Due to their high specific impulse, Hall thrusters are ideal low thrust devices for long missions such as satellite station keeping and deep space exploration. In Hall thrusters, the acceleration of ions by an electric field generates thrust. The electrons circulating between an external hollow cathode and an anode at the beginning of the channel maintain a specified potential drop corresponding to the discharge voltage. A radial magnetic field magnetizes the electrons causing an $\mathbf{E} \times \mathbf{B}$ Hall current to restrain the flow of electrons leading to a region of high ionization and strong electric field.

One motivation for developing a Hall thruster simulation is to construct an accurate model of the time-evolution of the channel walls due to erosion by energetic particles. The erosion of the Hall thruster channel walls is caused by sputtering due to ions and neutrals, and is a significant factor in determining operational lifetime. Since future missions will require thruster lifetimes on the order of several years, determining this lifetime experimentally in ground test facilities is both time-consuming and expensive, especially when attempting to optimize operating conditions or geometry for maximum life. A robust and accurate numerical simulation is a necessary alternative for evaluating performance and lifetime. In the present work, a sputtering model has been introduced into a two-dimensional (2D) hybrid Particle-In-Cell (PIC) simulation in order to determine the amount of erosion on channel walls of a laboratory Hall discharge. The effect of charge-exchange collisions and momentum-exchange collisions on the sputtering process has been investigated. In addition, a sheath model has been added and takes into account the acceleration effect of the wall potential on ions which scatter with the channel walls. While this present model assumes a static, imposed magnetic field, from the output of the simulation, we have calculated the induced magnetic field using a commercial finite element solver -Finite Element Method Magnetics (FEMM). The intent is to understand the effects of the induced field generated by an azimuthal drift in the thruster on the distortion of the potential distribution, and the ion trajectories. Finally, successive simulations of a more developed erosion model able to update the geometry of the channel walls, provides a good approximation of the erosion evolution of the channel walls for more than 2000 hours.

II. Numerical Model

A. Main Model

In order to obtain a better understanding of Hall thruster physics, a 2D (radial-axial or r-z) hybrid particle-in-cell (PIC) model has been developed at Stanford University by Fernandez et al.¹ This model was inspired by the model of Fife² and is described in more detail by Allis et al.³ In this hybrid model, the electrons are treated as a quasi-one-dimensional fluid governed by a generalized Ohm's law, and the ions and neutrals are described as discrete particles advanced in space using a PIC approach. An important element in the model is the ability to account for the finite-rate ionization processes, which depends critically on the computed electron temperature. The transient spatially varying electron temperature profile is calculated at each timestep by solving the following electron energy equation:

$$\frac{\partial}{\partial t} \left(\frac{3}{2} n_e k T_e \right) + \frac{\partial}{\partial \hat{n}} \left(\frac{5}{2} n_e v_{en} k T_e - K \frac{\partial T_e}{\partial \hat{n}} \right) = -\dot{n}_e \Phi(T_e) E_i - \alpha T_e^{3/2} + j_{en} E_{\hat{n}} \quad (1)$$

Here, K is the thermal diffusivity, which incorporates an anomalous electron transport coefficient. The ion production cost, $\Phi(T_e)$, is determined from the exponential expression given by Dugan⁴, and is evolved in the original nonlinear form. The terms on the right hand side of Eq. (1) represent the ionization and wall damping sink terms and the joule heating source term. In this equation, an experimentally based effective mobility is imposed to account for the anomalously high electron transport across magnetic field lines.⁵

In this model it is assumed that all ions created from ionization are singly charged, and the effect of the azimuthal current on the magnetic field within the channel is neglected. The constant magnetic field used as an input into the code is based on experimental measurements made in the Hall thruster channel with no plasma (and no azimuthal current). It is noteworthy that the induced magnetic field generated by the azimuthal current when the discharge is on can be as much as 5-10% of the static magnetic field. Although future simulations will account for this induced magnetic field, the final erosion results presented here neglect this induced field.

The computational geometry used in the simulation corresponds to the Stanford Laboratory Hall Thruster which has an 8 cm long and 1.2 cm wide channel, in a 9 cm (outer diameter) annulus. The computational domain extends from the anode, through the interior channel, and into the near field plume region. The computational grid, as shown in Fig. 1, consists of 101 grid points in the axial direction and 13 grid points in the radial direction.

In order to reduce the computational time, ions and neutrals are regrouped into macroparticles of varying sizes, which are spread over the computational grid cells. The simulation is initialized with about 500,000 neutral macroparticles, and about 350,000 ion macroparticles. When striking the walls, neutrals are diffusely scattered back into the channel using a Maxwellian distribution, whereas ions are assumed to recombine into neutrals and scatter diffusely.

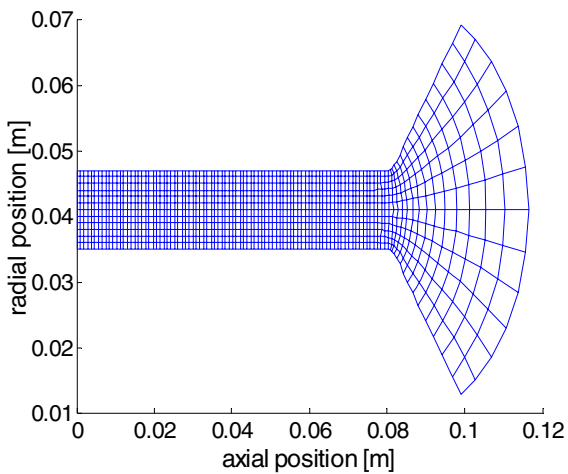


Figure 1. Computational grid of Stanford Hall thruster radial-axial simulation.

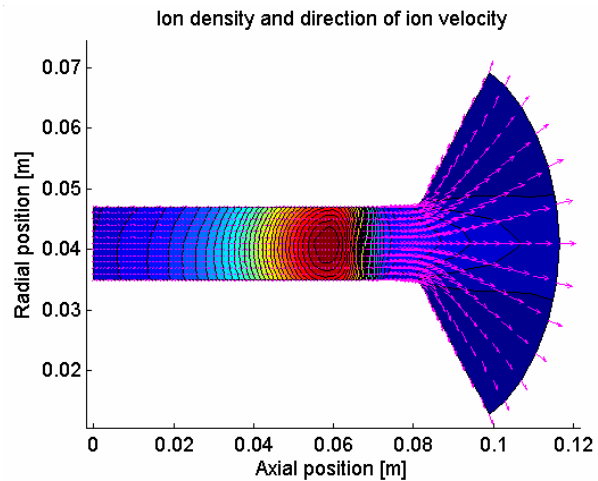


Figure 2. Computed ion density and ion velocities.

The ion and neutral timestep has been fixed at 25 ns whereas the electron timestep is on the order of 0.1 ns. The total amount of simulated time is 625 μ s which takes one day to run on a single processor (AMD Athlon 64 – 3500 MHz) desktop computer. Representative results of ion density distribution (color map) and ion velocity (superimposed vectors) averaged over time are illustrated in Fig. 2. An examination of Fig. 2 indicates that the plasma density is highest at about 2 -3 cm upstream of the exit of the channel. However, as shown below, erosion takes place mainly in the last 1 cm of the channel, due to the necessity to accelerate the ions to energies that are above the erosion threshold for the particular wall material, as discussed in the section below.

B. Sputtering Model

Sputtering is a physical phenomenon where atoms of a solid target are ejected due to the bombardment by heavy particles that have enough kinetic energy to overcome the inter-atomic binding energy of the bonded atoms of the target's surface. In the model, the target is the ceramic insulating material which constitutes the walls of the thruster.

Sputtering is largely driven by momentum exchange between the energetic particles and the atoms of the wall. The number of atoms ejected from the surface per incident particle is called the sputter yield, and it is an important measure of the efficiency of the sputtering process. The sputter yield primarily depends on the incidence angle and energy of the incident particle, the masses of incident and target particles, and the binding energy of atoms in the walls.

The sputter yield determined in the model is defined for each position z on the walls by:

$$S(z) = \hat{S}(\varphi) \cdot h(z, \varphi, \varepsilon) \cdot S(\varepsilon) \quad (2)$$

Here, $\hat{S}(\varphi)$ and $S(\varepsilon)$ are, respectively, the normalized sputter yield angular dependence (Fig. 3) and the sputter yield energy dependence as discussed by Manzella et al.⁶, and $h(z, \varphi, \varepsilon)$ is the normalized distribution function of the incident particles which play a role in the sputtering process. The distribution function is calculated at each wall position in z . Only ions with energy greater than a threshold energy of 50 eV and neutrals with energies greater than 60 eV (the energy threshold of ions plus the ionization energy of the atom) are considered in the sputtering process, as particles with energy less than the threshold energy are unable to break the bonds between the atoms in the ceramic walls.

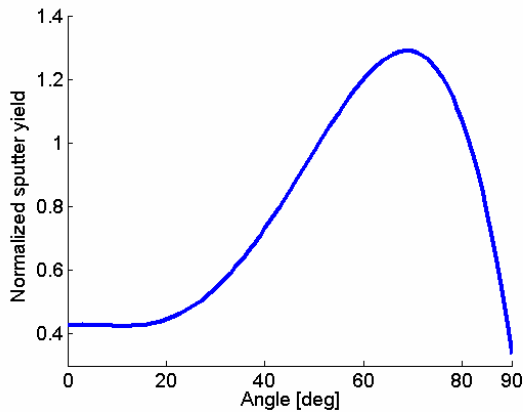


Figure 3. Normalized sputter yield angular dependence for xenon on boron nitride [see Ref. 6].

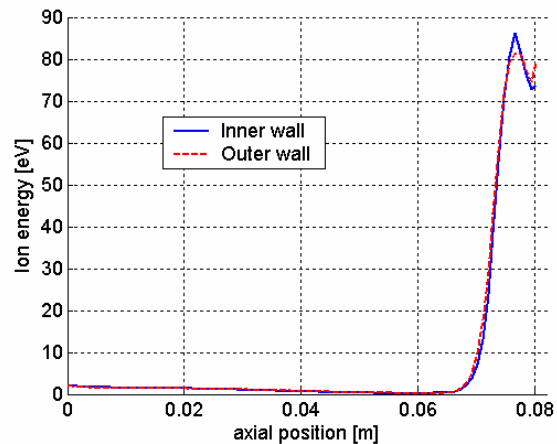


Figure 4. Average ion energy on the channel thruster walls.

The sputtering model has been integrated into the thruster simulation as follows. Particles positions and velocities are updated for each time-step using a leap-frog method. The model then checks the particle locations. If a particle is found outside of the boundaries of the computational grid, the position where the particle collided with the wall is determined if such a position exists (i.e., some particles may exit the computational boundaries in the plume without having collided with the wall). The energy and incidence angle of the impacting particles are then calculated to determine whether or not the particle contributes to the sputtering process. The sputter yield is determined, and the overall instantaneous (local) sputter rate is calculated from the rate at which these particles collide with the surface (wall ion current).

After a preliminary evaluation of the sputter yield using the simulation, it has been observed that nearly all of the erosion process, due to high energy ions, occurs in a region very near the thruster exit. This is confirmed by examining the ion energy distribution along the walls (Fig.4). A peak in ion energy is clearly observed on both walls in a region close to the channel exit. Therefore the present work focuses on studying the sputter yield in this region. In order to do this, the 1 cm long region where sputtering occurs, was divided into 45 segments, each one of them corresponding to an axial position along the walls. At each position, the model calculates the distribution function of the high energy particles impacting the walls and deduces the sputter yield from this distribution.

To update the shape of the channel walls, the radial positions of the nodes of the extreme radial grid lines (number 1 and 13) are modified depending on the instantaneous erosion rate calculated by the model. In order to make the computations tractable at this time, it is assumed that the discharge properties as determine in the originally non eroded geometry do not change. That is, the erosion process is assumed to not affect the discharge

operation. This assumption may be particularly severe when through-insulator erosion takes place and when the plasma begins to erode the actual magnetic pole piece. It is suspected however, that the recession of the ceramic walls plays only a minor role on the gas physics within the discharge. Future studies will however, confirm this conjecture. Another simplifying assumption in this preliminary version of the simulation is that only macroparticles are tracked into the expanded region, and the main characteristics of the eroded wall (potential, electron temperature, magnetic field, etc.) are assumed to be the same as those at the original (un-eroded) walls.

C. Ion-Neutral collisions

There are two types of collisions which have been included in the simulation: charge-exchange collisions and momentum-exchange collisions. The first type is found to have a significant effect on the simulation results, since charge-exchange collisions alter the velocity (energy) distribution of the ions and neutrals. During a charge transfer event, a slow neutral and a fast ion will respectively become a fast neutral and a slow ion. Elastic momentum-exchange collisions do not appear to significantly influence the simulation, but were included here to understand their role in altering the sputtering process. Elastic scattering between heavy particles results in a change in the direction of the particles. This change in direction modifies the angle of incidence of the ions scattering with the walls. Since neutrals are much slower than ions, the importance of elastic momentum-exchange collisions increases, especially in the last centimeter before the thruster exit, where the erosion process is prevalent.

As mentioned previously, the simulation uses a grid of cells where ions and neutral molecules are grouped into macroparticles. The probability of collision in each cell is determined by the No-Time-Counter (NTC) method of Bird.⁷

For each time-step the following number of pairs are selected in each cell:

$$\frac{1}{2} n_n n_i (\sigma_T * g)_{\max} * V_{cell} * dt \quad (3)$$

Here n_n and n_i are the neutral density and ion density, respectively. $(\sigma_T * g)_{\max}$ is the maximum value of the product between the collision cross-section and the relative velocity for all possible particle pairs. V_{cell} is the volume of the cell, and dt is the time-step. Differing macroparticle weights are accounted for in choosing collision pairs.

The probability of a collision for each selected pair is defined by:

$$P = \frac{\sigma_T * g}{(\sigma_T * g)_{\max}} \quad (4)$$

The experimental measurements of Pullins et al.⁸ are used to determine the total charge-exchange cross section as a function of energy:

$$\sigma_T = (-23.3 \log_{10}(g) + 188.81) \times 1.1872 \text{ \AA}^2 \quad (5)$$

Here σ_T is the total charge exchange cross section and g is the relative speed. The cross-section used for elastic collisions is that of Boyd and Dressler:⁹

$$\sigma_T(Xe, Xe^+) = \frac{6.42 \times 10^{-16}}{g} \text{ m}^2 \quad (6)$$

1. Charge-Exchange collisions

On average, a neutral macroparticle is two orders of magnitude larger than an ion macroparticle. Therefore, if a charge exchange collision is determined to take place, the larger particle (typically the neutral) is divided into a small particle the size of the collision partner and a larger particle containing the balance of the atoms/ions. Since the most probable scattering event involves very little momentum transfer, the pre-collision velocities of the ion and neutral macroparticles of the same size are exchanged while the remainder of the larger macroparticle keeps the same pre-collision velocity as it is assumed to not be subjected to a collision. Although this process removes fast ions which may contribute significantly to the sputtering process, it produces high energy neutrals which may also play a role in the erosion process and cannot be neglected. Fig. 5 shows that with charge-exchange collisions, the ion energy distribution is shifted towards lower energies near the exit. Fig. 6 shows that with charge-exchange collisions, the ion density near the walls decreases. This decrease in ion density is associated with decrease in

neutral density, since the neutral velocity increases due to charge-exchange collisions between slow neutrals and energetic ions.

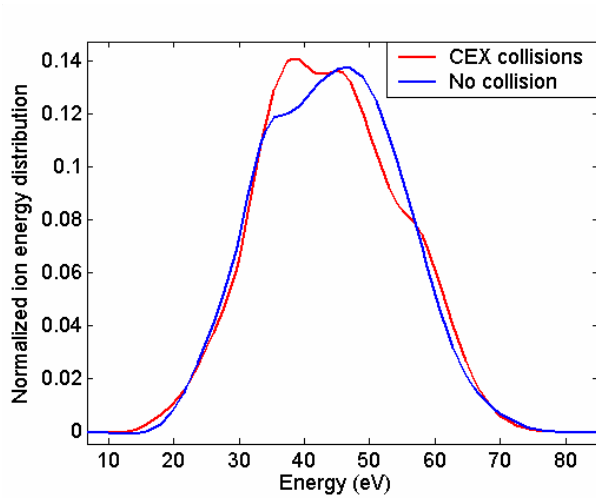


Figure 5. Energy distribution on the outer wall for a position located 7 mm before the exit plane.

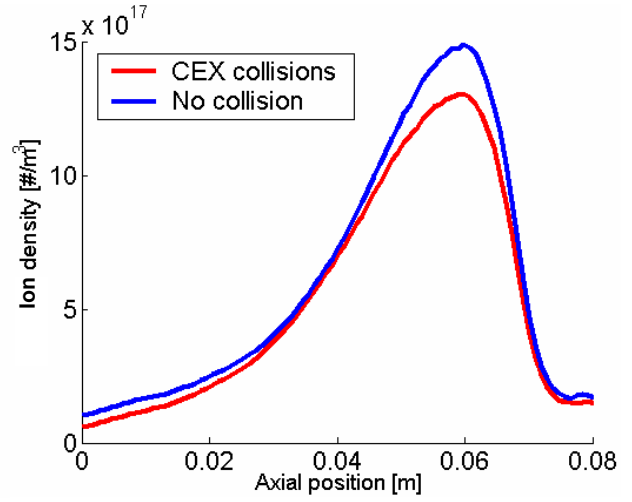


Figure 6. Ion density on the outer wall

2. Momentum-Exchange collisions

Similar to the treatment of charge-exchange collisions, for momentum-exchange collisions the larger macroparticle is divided into two smaller macroparticles, where one particle is the same size as its collision partner.

Momentum and energy are conserved in an elastic collision. The center of mass velocity \vec{v}_m and the magnitude of the relative velocity g are conserved quantities given by:

$$\begin{aligned}\vec{v}_m &= \frac{m_i}{m_i + m_n} \vec{v}_i + \frac{m_n}{m_i + m_n} \vec{v}_n \\ \vec{g} &= \vec{v}_i - \vec{v}_n \\ g^* &= g\end{aligned}\tag{7}$$

where $m_i, \vec{v}_i, m_n, \vec{v}_n$ respectively are the mass and the pre-collision velocities of the ion and neutral macroparticles, and g^* is the post-collision relative speed.

A variable hard sphere (VHS) model is used to describe the collision process. For the VHS model, the scattering angle χ is chosen as: $\cos \chi = 2\beta - 1$

Here β is a number randomly chosen between 0 and 1. The two particles undergoing the collision are assumed to have a trajectory in the 2D (\vec{z}, \vec{r}) plane.

The post-collision relative velocity is given by:
$$\vec{g}^* = \vec{g} \begin{bmatrix} \cos \chi \\ \sin \chi \end{bmatrix}\tag{9}$$

The post-collision velocities of the colliding particles are given by:

$$\begin{aligned}\vec{v}_i^* &= \vec{v}_m + \frac{m_n}{m_n + m_i} \vec{g}^* \\ \vec{v}_n^* &= \vec{v}_m - \frac{m_i}{m_n + m_i} \vec{g}^*\end{aligned}\tag{10}$$

3. Effects of collisions on thruster performance

The first effect of collisions on the thruster performance is a reduced thrust compared to a model with no collisions (Fig.7). This is mainly due to the fact that charge-exchange collisions decrease the number of fast ions which produce the thrust.

Momentum-exchange collisions might also lead to a change in the thrust. Since momentum exchange collisions modify the direction of ion velocity, the axial component of velocity, which contributes to the thrust, is altered. However this effect can occur in both ways: the axial velocity may decrease or increase. Therefore the global impact of elastic collisions on performance seems to be negligible.

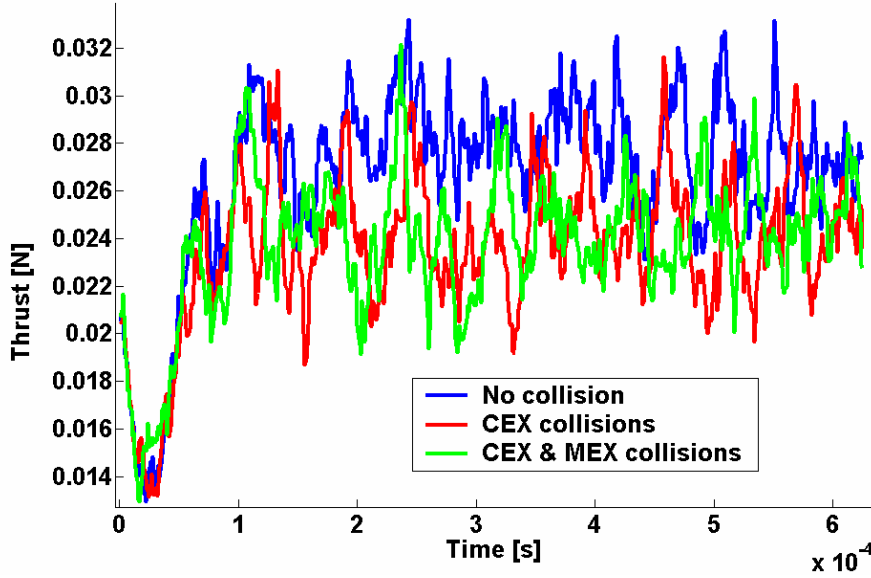


Figure 7. Computed thrust over time.

D. Sheath model:

When ions and electrons strike a wall, they recombine and are lost. Since electrons have greater velocities than ions, they leave the plasma faster than ions and collect on the walls^{10, 11}. This phenomenon creates a negative potential on the walls which repels electrons and attracts ions. In order to produce a steady state, ions and electrons must reach the walls at a rate equal to that at which they are formed. In our simulations, the grid is too coarse to adequately capture the wall pre-sheath (of course, the quasi-neutral assumption precludes capturing of any space charge within the sheath), and so the Bohm condition that must be established at the boundary between the bulk plasma and the sheath edge also may not be satisfied. Not accounting for the existence of a sheath therefore underestimates the incident ion energy. In order to take into account the effects of the sheath on the energy of the incoming ions with the walls, a simple sheath model has been added in the erosion calculation. This consists mainly of determining the potential drop in the sheath^{12, 13} by:

$$\Delta\phi_{wall} = -\frac{kT_e}{e} \ln \left[(1-\sigma) \sqrt{\frac{M_{Xe}}{2\pi M_e}} \right] \quad (11)$$

where σ is the total secondary electron emission yield given by:

$$\sigma = \sigma_0 + \frac{E_e}{E^*} (1-\sigma_0) \quad (12)$$

and E_e is the average energy of an incident electron given by:

$$E_e = \frac{3}{2} \frac{kT_e}{e} \quad (13)$$

Once σ reaches the value of 0.983 for xenon¹³, a potential well forms close to the wall which traps a fraction of the secondary electrons. Equation (11) is no longer valid and the new charge saturation regime is characterized by:

$$\Delta\phi_{wall} = -1.02 \frac{k T_e}{e} \quad (14)$$

As for the energy of the ions scattering with the insulator channel walls, we define:

$$E_{Xe^+} = \frac{v_{Xe^+}^2 M_{Xe}}{2} - e\Delta\phi_{wall} \quad (15)$$

It is then assumed that the potential drop of the sheath acts on the radial component of the velocity of the ions scattering with the walls. The velocity components at the wall of these ions are then defined by:

$$\begin{aligned} v_{z \text{ with sheath}} &= v_{z \text{ no sheath}} \\ v_{r \text{ with sheath}} &= \sqrt{\frac{2e}{M_{Xe}} \Delta\phi_{wall} + v_{r \text{ no sheath}}^2} \end{aligned} \quad (16)$$

III. Results and discussion

Based on the sputtering model, an erosion rate has been obtained for the neutrals (Fig.8) and for the ions (Fig.9) when charge-exchange collisions are taken into account. The sputtering due to energetic neutrals appears to be about one thousand times smaller than the rate of sputtering due to ions. As a result, the following discussion about wall sputtering and erosion focuses mainly on the role played by energetic ions.

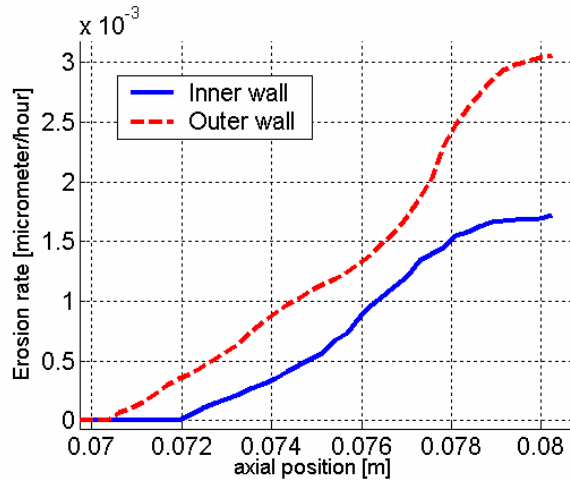


Figure 8. Neutral xenon contribution to the sputter rate.

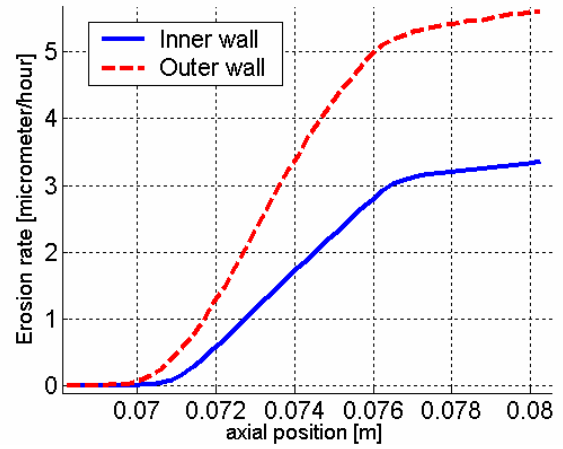


Figure 9. Xenon ion contribution to the sputter rate.

It is apparent from Fig. 9 that sputtering is more prevalent on the outer wall than on the inner wall, suggesting that if the wall thickness is comparable, through-wall erosion would take place first on the outer wall. At present, the primary reason for this asymmetry in the erosion has not yet been identified. To understand the origin for this asymmetry, which is likely to be traced back to the magnetic field distribution within the channel, we must understand the nature of the trajectory of ions as they accelerate through the potential distribution from the time and position at which they are born. It is noteworthy, however, that the potential contours are not only affected by the magnetic field distribution, but also by the plasma density distribution, and by gradients in the electron temperature..

In order to determine the local, instantaneous erosion rate, the wall ion flux is calculated from the ion velocity v_i and the ion density N_i at the walls:

$$J_i(z) = e N_i(z) v_i(z) \quad (11)$$

The erosion rate at each location on the wall is obtained by multiplying the ion flux on the wall by the sputter yield:

$$\frac{dr}{dt}(z) = S(z) \cdot J_i(z) \quad (12)$$

This erosion rate is presented in Fig. 10 accounting for the affect of charge-exchange and momentum-exchange collisions. The erosion rate increases rapidly with position until approximately 4 mm from the exit plane where it reaches a maximum level. In the simulation, it is found that the computed local sputter rate decreases slightly in the last 1-mm, due to edge-effects associated with the discrete nature of the domain in the very last computational cell in the channel. This decrease is ignored in the calculation of the erosion rate, as it is assumed that the resulting wall profile could not be supported by the near-normal incidence of the ion beam. More importantly, it is noted that a general consequence of charge-exchange collisions is that they reduce the maximum erosion rate by more than a half micrometer per hour (~ 20%), while momentum-exchange collisions increase the erosion rate slightly. This increase is due to the collisional redirection of ions (accelerated primarily along the axial direction) towards the walls.

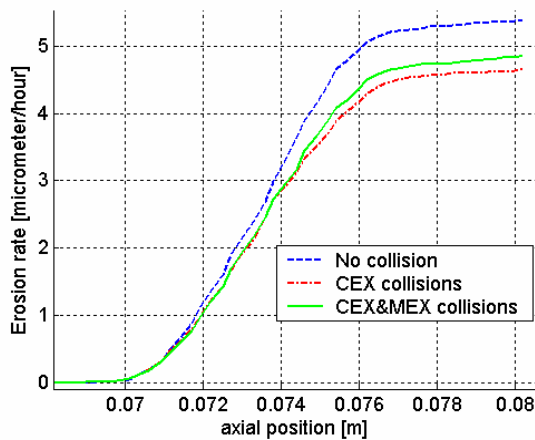


Figure 10. Wall erosion rate on the outer wall.

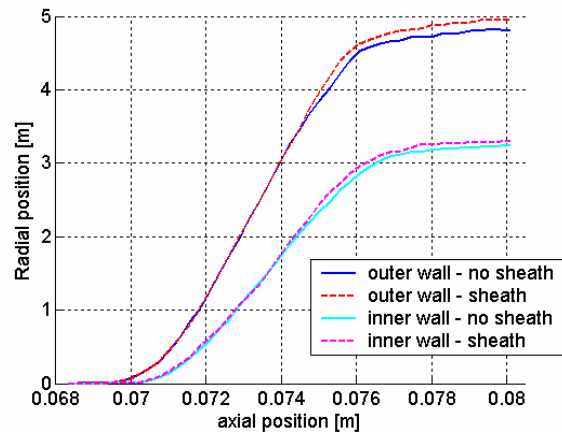


Figure 11. Erosion rate on the walls with and without the sheath model.

In order to assess the impact of the plasma sheath, the simulated erosion rate was calculated with and without a sheath model. As shown in Fig. 11, including the potential drop in the sheath slightly increases the erosion rate. The presence of a sheath increases the number of high energy ions, but it also modifies the incidence angle of those ions scattering with the walls. However, in order to have an accurate model of the thruster physics, future simulations will continue taking into account the presence of a sheath.

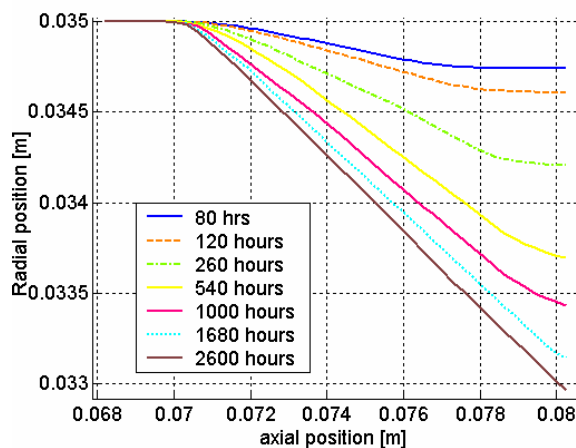


Figure 12. Simulation of the erosion on the inner wall.

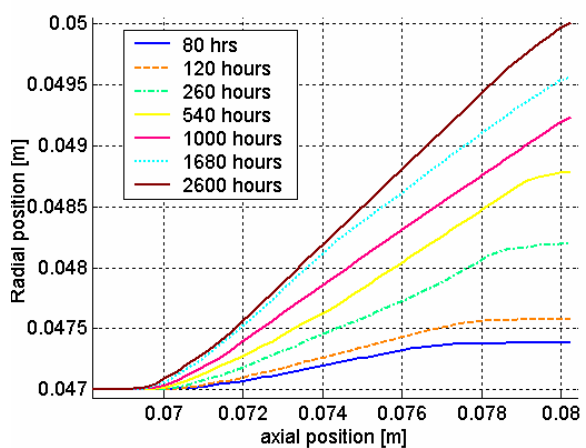


Figure 13. Simulation of the erosion on the outer wall.

Figures 12 and 13 present an estimation of the erosion history of the inner and outer thruster walls. The simulations are carried out to an effective thruster operating time of 2600 hours. It is observed that the erosion rate decreases substantially over time, with more than half of the erosion occurring in the first 500 hours of life. This result is in qualitative agreement with similar calculations using 1-D plasma flow models although on a considerably different thruster⁶. This drop in the instantaneous erosion rate is believed to be mainly due to the angular dependence in the sputter yield (Fig. 3), which implies that the majority of high energy ions contributing to sputtering have incident angles greater than 60° relative to the surface normal. It is noteworthy that by 2600 hours, the surface is predicted to erode to an angle of about 17° relative to the thruster axis.

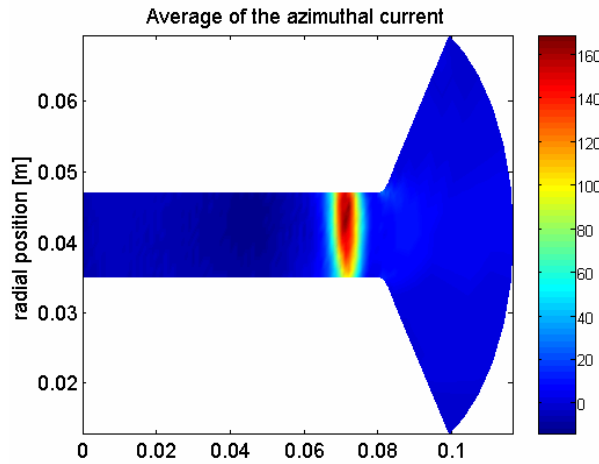


Figure 14. Azimuthal current density from the code.

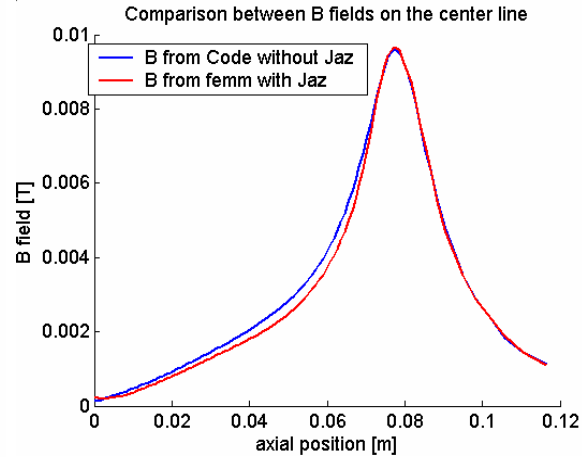


Figure 15. Comparison between magnetic fields with and without azimuthal perturbations.

In the simulation described above, the affect of the induced azimuthal current on the discharge is ignored as it is in most, if not all, 1D and 2D ($r - z$) simulations of Hall thrusters. In the preliminary study described below, we examine the possible affect if any, that the induced current may have on altering the trajectories of the ions, since in our case, the azimuthal Hall current is estimated to be about 10A.

We can use the output of the simulation to predict the azimuthal current density by the following approximate expression:

$$J_{e\theta} = en_e \frac{E_z}{B_r} \quad (16)$$

The computed azimuthal current density is shown in Fig. 14. It is noteworthy that this computed current density is about a factor of three or more lower than recent measurements made in our laboratory, using a non-intrusive antenna and fast current interruption¹⁴. Despite this difference, we have used this azimuthal current density together with the Finite Element Method Magnetics (FEMM) software package¹⁵ to predict the induced magnetic field that can be expected, to first order. A comparison is made in Fig. 15, of the original externally-imposed magnetic field, and the first-order correction to the field, to account for this azimuthal current. Our preliminary findings indicate that this adjustment in the magnetic field has only a minor affect on the computed wall erosion. However, as the predictive capability of the simulation improves, and if it is indeed able to better predict the higher Hall currents (and hence stronger perturbation to the magnetic field), a better understanding of the significance of its importance in erosion will be obtained. The role of the induced magnetic field on the plasma structure and erosion behavior is the subject of ongoing studies.

IV. Conclusion

We present the results of numerical studies aimed at understanding the evolution of the erosion process in a Hall thruster channel. We have incorporated a model of ion and energetic neutral-induced sputtering a 2D hybrid PIC simulation. The hybrid PIC simulation includes charge-exchange and momentum-exchange collisions as the former is found to have a significant effect on the instantaneous wall erosion rate. The results of our study conclude that energetic neutrals can be formed through charge exchange processes, but they seem to have a negligible impact on the overall sputtering/erosion process. Charge-exchange collisions appear to result in a reduction in the erosion rate and also a reduction in the thruster performance. Momentum-exchange collisions appear to have less significance in the wall erosion process. The role of the sheath has been added in a simple fashion, in the acceleration of ions in the radial direction, and it is found that it does lead to a slight increase in the erosion rate. A Preliminary study of the possible affect on erosion that the induced magnetic field due to the azimuthal (Hall) current has, seems to suggest that this effect may be small. However, it was noted that the simulation under predicts the Hall current (when compared to recent measurements), and so broad conclusions regarding this phenomenon cannot be made at this time.

Future work will focus on developing a more refined model of the erosion history through successive discharge simulations accounting for the effect that the advanced (eroded) channel walls has on the overall discharge properties. Furthermore, improvements will also be made to the description of the charge-exchange process to account for the angular dependence of the scattering process (differential scattering). Finally, as the model improves, we will be in a better position to address the significance that the induced current plays on altering the magnetic field profile and ion trajectories. The overall objective is to improve the overall robustness of these simulations so that they may become useful in predicting long-term thruster behavior and thruster lifetime for specific thruster geometries.

Acknowledgments

This work was supported by the Air Force Office of Scientific Research. Support for E. Sommer was provided by SNECMA.

References

- ¹Fernandez, E., Cappelli, M. A., Mahesh, K., "2D Simulations of Hall Thrusters," *CTR Annual Research Briefs*, 1998, pp. 81.
- ²Fife, J. M., "Nonlinear Hybrid-PIC Modeling and Electrostatic Probe Survey of Hall Thrusters," Ph.D. Dissertation, Aeronautics and Astronautics Dept., Massachusetts Institute of Technology, Cambridge, MA, 1998.
- ³Allis, M. K., Gascon, N., Vialard-Goudou, C., "A Comparison of 2-D Hybrid Hall Thruster Model to Experimental Measurements", 40th AIAA/ASME/ASEE Joint Propulsion Conference, Ft. Lauderdale, FL, July 11-14, 2004.
- ⁴Dugan, J. V. and Sovie, R. J., "Volume Ion Production Costs in Tenuous Plasmas: A General Atom Theory and Detailed Results for Helium, Argon and Cesium," NASA TN D-4150.
- ⁵Fernandez, E., Borelli, N., Cappelli, M. A., Gascon, N., "Investigation of Fluctuation-Induced Electron Transport in Hall Thrusters with a 2D Hybrid Code in the Azimuthal and Axial Coordinates", 45th Annual Meeting of the Division of Plasma Physics, Albuquerque, New Mexico, October 27-31, 2003.
- ⁶Manzella, D., NASA Glenn research Center, Cleveland, OH 44135, Yim, J. and Boyd, I., University of Michigan, Ann arbor, MI 48109, "Predicting Hall Thruster Operational Lifetime", AIAA-2004.
- ⁷Bird, G. A., "Molecular Gas Dynamics and the Direct Simulation of Gas Flow", Oxford Science Publication, Ch.2&11, 1994.
- ⁸Pullins, S., Chiu, Y., Levandier, D. and Dressler, R., "Ion Dynamics in Hall Effect and Ion Thrusters: $Xe^+ + Xe$ Symmetric Charge Transfer," *AIAA Paper* 00-0603, Jan. 2000.
- ⁹Boyd, I. D., Dressler, R. A., "Far Field Modeling of the plasma Plume of a Hall Thruster", *Journal of Applied Physics*, Vol.92, nb 4, pp.1764-1774, 2002 August 15.
- ¹⁰Chen, F., F., *Introduction to Plasma Physics*, Press, New York, pp-244-247, 1974.
- ¹¹Guthrie, A., Wakerling, R. K., *The Characteristics of Electrical Discharges in Magnetic Fields*, McGraw-Hill Book Company, New York, Ch. 3, 1949.
- ¹²Barral, S., Gascon, N. and Dudeck M., "Wall material effects in stationary plasma thrusters. II. Near-wall and in-wall conductivity", *physics of plasmas*, Vol.10, Nb.10, pp 4137-4152, Oct. 2003
- ¹³Taccogna, F., Longo, S. and Capitelli M., "Plasma sheaths in Hall discharge", *physics of plasmas*, Vol.10, 2005
- ¹⁴Thomas, C. A., Gascon, N., Cappelli, M. A., "Non-Intrusive Characterization of the Hall Thruster Azimuthal Drift Current", 40th AIAA/ASME/ASEE Joint Propulsion Conference, Ft. Lauderdale, FL, July 11-14, 2004.
- ¹⁵FEMM, Finite Element Method Magnetics, Software Package, Ver. 4.0, Foster-Miller, Inc., Boston, MA, 2004